Applied Physics Letters

RESEARCH ARTICLE | MAY 20 2025

# Reconfigurable phase-change metasurface for multifunctional control of chiral emission

Cai Luo ; Nannan Hu; Jianmei Li ; Sha Hu ; Ziyi Fu ; Zhixiang Yu; Yanxue Hou ; Aizi Jin; Baogang Quan; Shibing Tian; Haifang Yang ; Geng Li; Xiaoyu Zhang ; Xiaofeng Fan ; Yang Guo ; Changzhi Gu



*Appl. Phys. Lett.* 126, 201705 (2025)
https://doi.org/10.1063/5.0267717









AIP Publishing

Applied Physics Letters ARTICLE pubs.aip.org/aip/apl

# Reconfigurable phase-change metasurface for multifunctional control of chiral emission

Cite as: Appl. Phys. Lett. **126**, 201705 (2025); doi: 10.1063/5.0267717
Submitted: 25 February 2025 · Accepted: 8 May 2025 ·
Published Online: 20 May 2025



Cai Luo,[1,2] Nannan Hu,[2,3] Jianmei Li,[1,a)] Sha Hu,[3] Ziyi Fu,[1,2] Zhixiang Yu,[1] Yanxue Hou,[1] Aizi Jin,[2] Baogang Quan,[2] Shibing Tian,[2] Haifang Yang,[2] Geng Li,[2,4] Xiaoyu Zhang,[5] Xiaofeng Fan,[5] Yang Guo,[2,6,a)] and Changzhi Gu[2,6,a)]

## AFFILIATIONS

[1]Key Laboratory for Microstructural Material Physics of Hebei Province, School of Science, Yanshan University, Qinhuangdao 066004, China
[2]Beijing National Laboratory for Condensed Matter Physics, Institute of Physics, Chinese Academy of Sciences, Beijing 100190, China
[3]College of Physics, Henan University of Technology, Zhengzhou 450001, China
[4]Songshan Lake Material Laboratory, Guangdong 523808, China
[5]Key Laboratory of Automobile Materials of MOE, College of Materials Science and Engineering, Jilin University, Changchun 130012, China
[6]School of Physical Sciences, CAS Key Laboratory of Vacuum Physics, University of Chinese Academy of Sciences, Beijing 100190, China

[a)]**Authors to whom correspondence should be addressed:** jianmeili@ysu.edu.cn; yangguo@iphy.ac.cn; and czgu@iphy.ac.cn

## ABSTRACT

In optoelectronics and photonics, developing multifunctional light-emitting devices has become a prominent research area. However, achieving integration of polarization control, intensity modulation, and tunability within a single device presents a formidable challenge. Here, we report the design and implementation of a symmetric bound state in the continuum (BIC) realized by a metasurface composed of perovskite nanobars on a silica substrate. Through the incorporation of both in-plane and out-of-plane symmetries, the BIC undergoes a transformation into a chiral quasi-bound state in the continuum (q-BIC). The chiral q-BIC metasurface exhibits an intrinsic chiral response, characterized by nearly perfect circular dichroism of 0.96, a key property for chiral optical applications. Furthermore, the integration of $Sb_2S_3$ phase-change materials into the metasurface enables dynamic regulation of resonant circularly polarized emission wavelengths between 760 and 820 nm, with selective enhancement of right circularly polarized emission by 240-fold and suppression of left circularly polarized emission. Our chiral q-BIC metasurface enables single-device multi-function integration, offering a versatile and dynamically tunable platform for enhanced chiral optical responses across optoelectronics and photonics.



In the rapidly advancing field of optoelectronics and photonics, the exploration of multifunctional light-emitting devices has attracted substantial attention. These devices, distinguished by their versatile functional attributes, possess significant potential for a wide range of applications.[1,2] Polarization control represents a critical aspect within the realm of multifunctional light-emitting devices. Circularly polarized (CP) luminescence, in particular, has emerged as a prominent research focus, owing to its potential utility in various domains such as information storage,[3] display technology,[4,5] biomedicine,[6] and quantum optics.[7] The unique optical properties of CP light offer an additional dimension of information, thereby facilitating the development of high-resolution and high-contrast optical devices and systems. However, traditional semiconductors commonly exhibit a lack of effective polarization control during the emission process.[8–10] This is primarily due to the typically isotropic nature of the electron transition process within these materials, which results in a uniform distribution of the polarization state of the emitted light.

Intensity control constitutes another crucial aspect of multifunctional light-emitting devices. These devices must possess the ability to precisely modulate the intensity of light emission, a requirement of utmost importance for applications that demand varying levels of brightness, such as display technology[11,12] and optical communication.[13] The quality factor (Q), a quantitative measure of resonant systems, plays a significant role in enhancing luminescence efficiency and

the sharpness of the optical response.[14,15] In addition to polarization and intensity control, tunability emerges as a key characteristic of multifunctional light-emitting devices.[16–18] Dynamic tunability and reconfigurability are indispensable for meeting the diverse requirements of these devices across different application scenarios. However, there is a lack of in-depth investigations into the integration of polarization control, intensity control, and tunability within a single device. The complex interplay among these functions, along with the necessity for precise control at the micro- and nano-scales, presents significant scientific and technological challenges. To address these challenges, a comprehensive understanding of the fundamental physical mechanisms underlying these phenomena is essential.

Metasurfaces, as innovative artificial micro-nano structured materials, hold great promise in precisely manipulating light–matter interactions. By designing their geometric shape, size, and material composition, flexible control over light propagation, polarization, and phase can be achieved, making them a promising candidate for realizing multifunctional light-emitting devices.[19,20] In particular, the dynamic tuning of metasurfaces has been realized through electrical doping,[21,22] liquid crystals,[23,24] and phase-change materials.[25] Nevertheless, two-dimensional (2D) planar metasurfaces are devoid of intrinsic chirality, a feature that is of utmost significance not only for the phenomenon of CP luminescence but also for the accurate detection and sophisticated manipulation of chiral biomolecules in various biological and chemical processes. The out-of-plane mirror symmetry of 2D planar structures limits the generation of intrinsic chirality and impedes the development of multifunctional light-emitting devices with efficient polarization control.[26–29] In contrast, three-dimensional (3D) structures have the potential to break mirror symmetry and introduce specific asymmetries in 3D space, thereby generating intrinsic chirality.[30–33] Despite the complexity of 3D structures and significant fabrication challenges,[34–36] achieving dynamic tunability and reconfigurability in 3D chiral metasurfaces remains challenging. Further research is needed to explore mechanisms that can respond to external stimuli such as thermal, mechanical, optical, and electric field control, and facilitate the adjustment of chiral structure and optical properties.

In this study, we propose a reconfigurable 3D high-Q chiral metasurface for efficient and dynamic control of CP luminescence in perovskite materials. Its unique design supports a bound state in the continuum (BIC) state, which enhances the Q-factor[37–39] and luminescence efficiency. Breaking 3D mirror symmetry induces intrinsic chirality, enabling selective interaction with CP light, which can be identified by circular dichroism (CD) of 0.96. By varying the ratios of amorphous and crystalline $Sb_2S_3$ phase-change materials, we showcase active tuning of CP emission wavelength from 760 to 820 nm, accompanied by a 240-fold enhancement in light emission intensity. Our work provides a foundation for integrating polarization, intensity, and tunability in a single device, with potential applications in sensing, communication, quantum computing, and displays.

The schematic diagram proposed in this study is illustrated in Fig. 1. The initial BIC metasurface is constructed based on a square-lattice periodic structure with lattice spacing *a*. Each unit cell comprises of two cuboid-shaped nanobars made of perovskite materials, characterized by the length (*L*), width (*W*), and height (*H*). The entire structure is supported on a silica substrate (refractive index

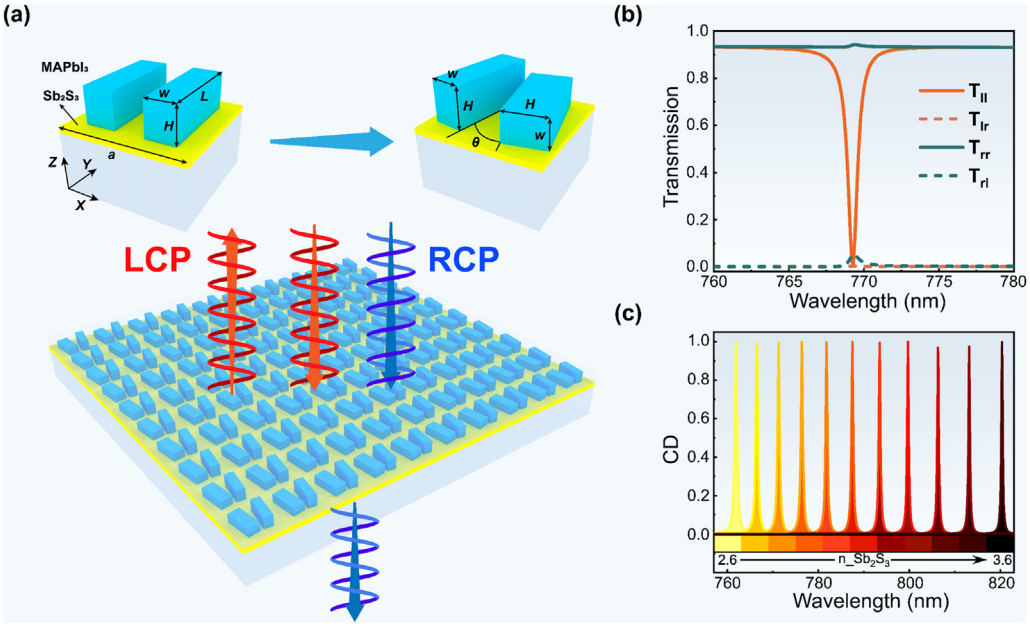


**FIG. 1.** Concept of the maximally chiral q-BIC metasurface. (a) Schematic diagram of the maximally chiral q-BIC metasurface. The inset shows the transition from BIC to chiral q-BIC, illustrating the specific structural parameters of the perovskite nanobars, the length (L), width (W), height (H), and the in-plane asymmetry parameter ($\theta$), respectively. (b) The RCP and LCP transmittance spectra measured at an in-plane asymmetry parameter $\theta = 8°$ with L = 310 nm, W = 100 nm, and H = 120 nm, maintaining a fixed height difference of d = H–W = 20 nm. At this time, LCP incidence exhibits strong field enhancement, while RCP incidence remains completely decoupled from the structure, thereby maximizing chirality generation. (c) The evolution process of the CD value of the structure with changes in the refractive index of the phase-change material $Sb_2S_3$, achieving near-unity CD across a broad spectral range of 760–820 nm.

$n_{sub} = 1.45$). A 20-nm-thick phase-change antimony trisulfide ($Sb_2S_3$) film is grown on it to introduce tunability, and subsequently covered with polymethyl methacrylate (PMMA, refractive index $n_{pmma} = 1.49$). The significant refractive index contrast caused by the structural phase transition of $Sb_2S_3$ [40,41] makes this structure create unique conditions for achieving tunable light polarization modulation. Due to the non-leaking characteristic of BICs, evidenced by a theoretically infinitely large Q-factor, this symmetric metasurface cannot effectively couple with the free light field. By introducing asymmetry parameters, specifically the included angle ($\theta$) and the height difference ($d = H - W$) between two nanobars [see Fig. 1(a) inset], which break the in-plane and out-of-plane symmetries, respectively, the primitive BIC metasurface can be transformed into the chiral quasi-bound state in the continuum (q-BIC) metasurface. Consequently, as shown in Fig. 1(b) chiral light–matter interactions have significantly enhanced the chiral response of perovskites, characterized by the transmission CD, defined as $CD = (T_{LCP} - T_{RCP})/(T_{LCP} + T_{RCP})$, where $T_{LCP}$ and $T_{RCP}$ are the transmission rates of left circularly polarized (LCP) and right circularly polarized (RCP) light, respectively. In Fig. 1(c), the chiral response of perovskites can be dynamically tuned from 760 to 820 nm, which aligns with a photoluminescence (PL) emission spectrum of $MAPbI_3$ [refer to Fig. S1(c)], by changing the refractive index of $Sb_2S_3$ from 2.6 to 3.6 [as seen in experimentally measured data in Fig. S1(a)] during phase transition. This perturbation affects only the resonant wavelengths without significantly modifying the main field patterns and corresponding chiral response.[42]

Figure 2 presents the simulated results of the symmetric BIC metasurface. The geometric parameters are $a = 420$ nm, $L = 330$ nm, $W = 100$ nm, and $H = 120$ nm, respectively. As illustrated in Fig. 2(a), the transmission spectra of the passive metasurface were calculated as a function of the in-plane rotation angle $\theta$, which serves as an asymmetry factor to convert non-radiative BIC into the leaky q-BIC. As the $\theta$ increases from 0° to 12°, the resonant position gradually undergoes a blueshift from 773 nm to around 765 nm. In Fig. 2(b), the Q-factor exceeds $10^7$ near 0° and decreases rapidly with increasing rotation angle. Due to the existence of out-of-plane symmetry, the metasurface does not exhibit a chiral response ($CD = 0$) as the rotation angle changes. The formation of the BIC mode in the symmetric structure is mainly attributed to the destructive interference between two parallel electric dipoles with opposite orientations.[33] As depicted in Fig. 2(c), the distribution of the electric field in the XY-plane reveals that two electric dipoles with opposite directions jointly form an electric quadrupole-like configuration with the $C_2$ symmetry. The transverse electric (TE) field arranges in a circular pattern, generating an out-of-plane magnetic dipole moment. The magnetic field is oriented along the Z-direction, which is perpendicular to the electric field. Previous studies indicate that optical activity, such as polarization rotation or chirality, cannot occur when the electric and magnetic fields are mutually perpendicular and lie on two orthogonal planes.[30,43,44] Under a configuration, the radiated fields are parallel, resulting in the absence of a chiral response.

To achieve a chiral q-BIC metasurface, we introduce both asymmetry parameters of the rotation angle $\theta$ and the height difference $d$

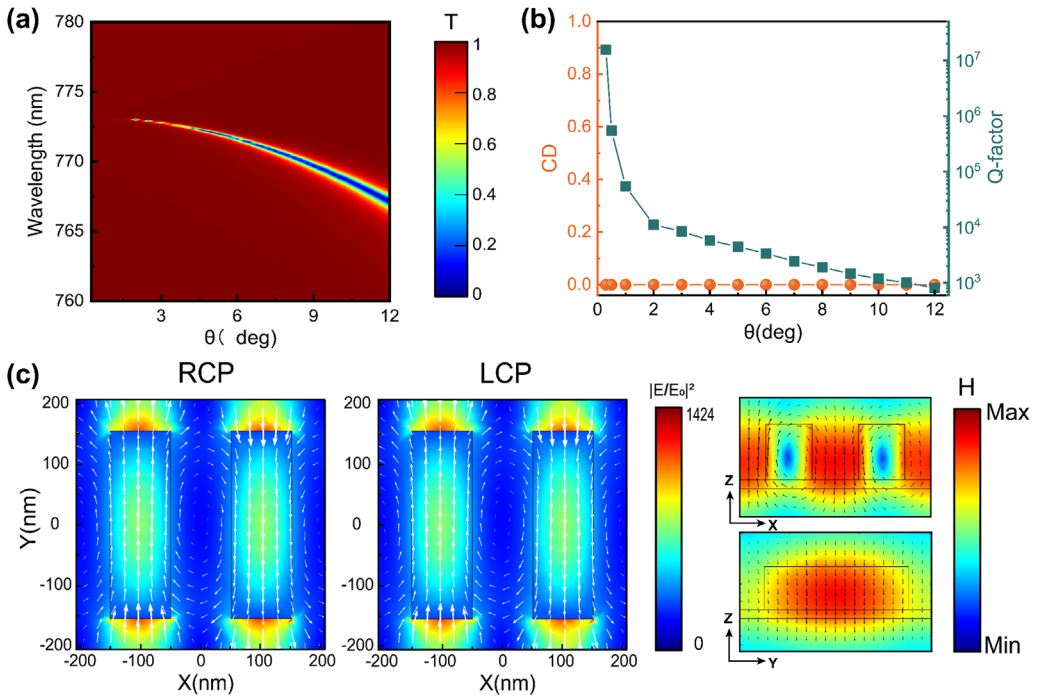


**FIG. 2.** The characteristics of the BIC supported by the parallel dielectric plate structure. (a) Simulation of the variation of the Y-polarized light transmittance spectrum with $\theta$ (shown on the color scale). The solid white circles denote the BIC. (b) The calculated CD (orange dots) and the corresponding fitted Q-factors (olive squares) as a function of $\theta$. (c) The electromagnetic distribution characteristics of the BIC. The electric field enhancement and the out-of-plane magnetic field distribution of the parallel dielectric rod structure under LCP and RCP incidence indicate that the BIC is in the transverse electric (TE) mode. The in-plane electric field is perpendicular to the out-of-plane magnetic field.

between two nanobars to break the in-plane and out-of-plane symmetries. The height difference of nanobars with rotation angle redistributes their fields and creates a vertical offset ($d$) between the two dipoles. The coupling parameters of LCP and RCP waves ($m_{\pm}$) to a metasurface are proportional to $\sin(kd/2 \mp \theta)$,[33] producing a chiral response (see the supplementary material for details). In Fig. 3(a), with the fixed height difference of $d = 20$ nm, as the rotation angle $\theta$ increases, the metasurface gradually decouples from the RCP, while strong resonance occurs for the LCP, thereby generating maximum chirality. The CD value gradually increases with rotation angle $\theta$ and reaches its maximum when the rotation angle $\theta = 8°$ [orange curve in Fig. 3(b)]. The breaking of the in-plane symmetry of the structure causes a sharp drop in the Q-factor [dark cyan curve in Fig. 3(b)]. When the angle $\theta$ is introduced, the $C_2$ symmetry of the in-plane electric field is broken, resulting in a non-zero average in-plane electric field. Upon introducing a height difference $d$, the circular electric field plane tilts, generating an out-of-plane electric field component. This, in turn, leads to the appearance of an in-plane magnetic field [Fig. 3(c)].

To further understand this phenomenon, we analyzed the chirality of the metasurface by calculating the reactive helicity density (RHD),[30,45,46] which is defined as $RHD = \frac{c}{\omega} Re(\boldsymbol{D} \cdot \boldsymbol{B}^*)$, where $\omega$ is the angular frequency of light, $\boldsymbol{D}$ is the electric displacement field, and $\boldsymbol{B}^*$ is the complex conjugation of magnetic flux density.[47] This optical chirality factor is typically normalized to the reference value using circularly polarized light. The RHD distribution in q-BIC metasurfaces with either in-plane or out-of-plane symmetry breaking exhibits antisymmetric characteristics [Figs. S4(a) and S4(b)]. However, in chiral q-BIC metasurfaces where both in-plane and out-of-plane symmetries are simultaneously broken, the near-field generates a non-equilibrium RHD distribution, corresponding to circularly polarized radiation in the far field, as shown in Fig. 3(d).

Subsequently, we turn to investigate the chiral optical response of the active metasurface. We calculated CP emission spectra using the reciprocity principal method (see the supplementary material for details), as depicted in Fig. 4. The degree of circular polarization (DCP) is defined as $\rho_c = (\hat{I}_{RCP} - \hat{I}_{LCP})/(\hat{I}_{RCP} + \hat{I}_{LCP})$, where $\hat{I}$ is the field enhancement factor. Compared to the symmetry-protected BIC metasurface [Fig. 4(a), top panel], the chiral q-BIC metasurface demonstrates significantly enhanced the LCP emission, while the RCP emission is almost completely suppressed, leading to a DCP close to unity [Fig. 4(a), bottom panel]. Figure 4(b) presents a direct comparison of field distributions under RCP and LCP incidences at the peak-enhanced wavelength from the bottom panel of Fig. 4(a). Compared with the field intensities in symmetry-protected BIC metasurfaces, the chiral q-BIC metasurface exhibits dramatically enhanced LCP field intensity while strongly suppressing RCP field strength. The field enhancement factor can be calculated with the temporal coupled mode theory, which can be expressed by the following equations: $Q_t/Q_r$, where $Q_t$ and $Q_r$ represent the total and radiative Q-factors, respectively. The high Q-factor of the q-BIC enables a significant enhancement of the CP field enhancement factor.

Figure 4(c) illustrates the simulated CP emission spectra with varying the ratios of amorphous and crystalline $Sb_2S_3$, consistently displaying an ultra-narrow full width at half maximum (FWHM) of 1.35 nm. The upper and lower parts represent the enhancement factors

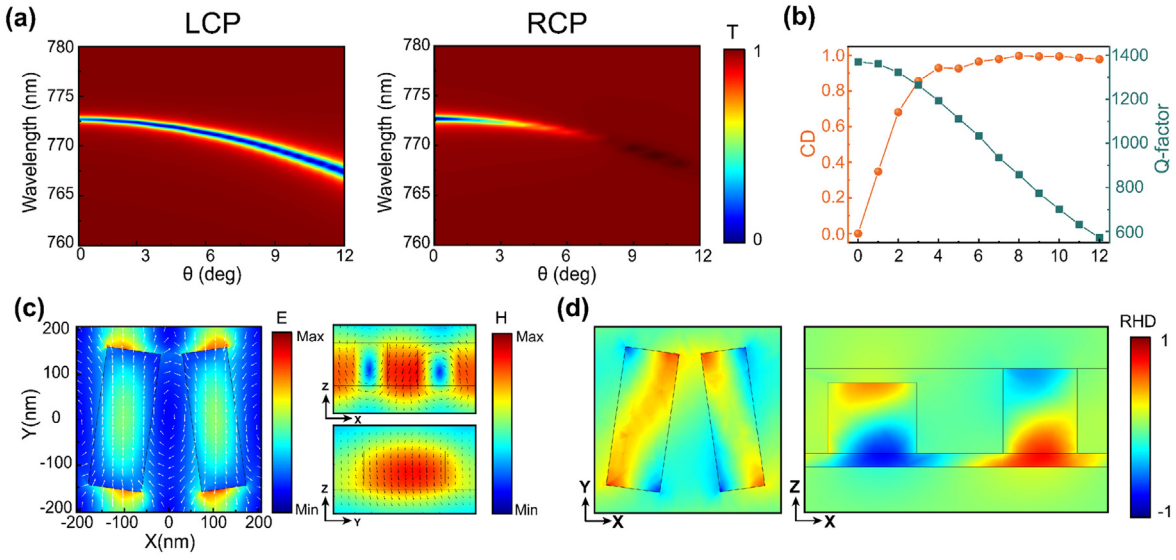


**FIG. 3.** Generation of maximum chirality. (a) When the height difference between the left and right dielectric rods is fixed at d, the simulated variations of the LCP and RCP transmittance spectra with $\theta$ (shown on the color scale) are presented. As the angle $\theta$ increases, RCP is completely decoupled from the structure. (b) The left part shows the calculated LCP and RCP transmittance spectra when the height difference is fixed at d and $\theta = 8°$. The position of the maximum chiral q-BIC is marked with a yellow background. The right part shows the calculated CD (orange dots) and the fitted Q-factors (olive squares) as a function of $\theta$ when the height difference is fixed at H–W. Maximum chirality occurs at $\theta = 8°$. (c) Electromagnetic distribution characteristics of the maximum chiral q-BIC. The in-plane symmetry breaking results in a component of the electric dipole in the X direction. The out-of-plane symmetry breaking causes the magnetic dipole perpendicular to the plane to tilt, and there is a magnetic dipole component in the in-plane X direction. (d) Near-field RHD distribution of the maximum chirality structure. In-plane and out-of-plane mirror symmetry breaking induces asymmetry in the near-field RHD within the dielectric rod, leading to a non-zero overall RHD.

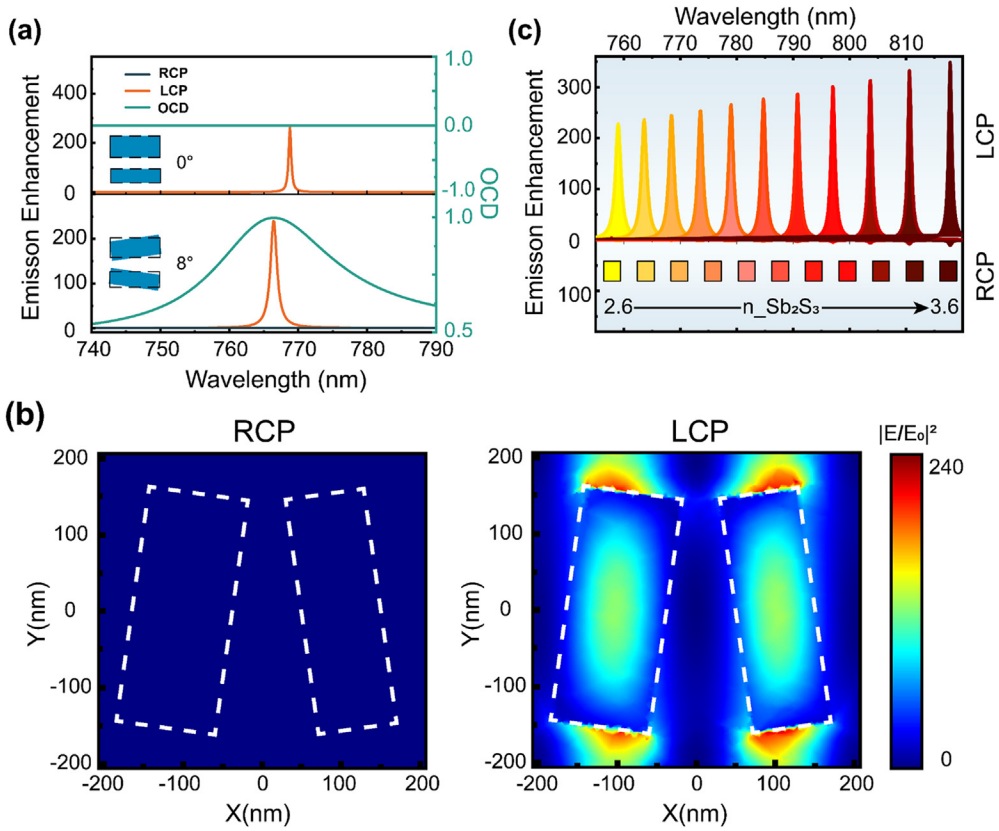


**FIG. 4.** Tunable maximum chiral emission achieved through chiral q-BICs. (a) Reciprocal calculations of emission enhancement when the rod inclination angles are 0° and 8° with a fixed height difference d. When the rotation angle of the dielectric rod $\theta = 0°$, the RCP and LCP emissions are identical (degree of circular polarization $\rho_c = 0$). However, in the tilted dielectric rod pair, the RCP emission is strongly enhanced while the LCP emission is almost completely suppressed, resulting in the degree of circular polarization approaching unity ($\rho_c \approx 0.96$). (b) Field profiles under RCP and LCP incidence at the peak enhancement wavelength in (a, bottom panel). The dielectric rod is indicated by a dashed box. (c) The evolution process of the reciprocal calculations of the LCP and RCP emission enhancements of the structure with the refractive index change of the phase-change material $Sb_2S_3$. DCP close to unity can be achieved in the wide spectral range of 760–820 nm.

of the LCP and RCP emission fields, respectively. During the phase transition of the phase-change material, the alteration in its refractive index affects solely the resonant wavelengths, rather than significantly modifying the main field patterns and their associated chiral response. The resonant CP emission can be effectively modulated, exhibiting a wavelength redshift from 760 to 820 nm while maintaining the maximal CD and strong emissions enhancement with over 240-fold circular polarization selectivity. This phenomenon implies that the crystallinity can be precisely tuned to continuously control the resonance peak within the operational bandwidth.

In summary, we have transformed a symmetric BIC metasurface into a chiral q-BIC metasurface through introducing 3D asymmetry parameters for in-plane or out-of-plane symmetry breaking. This high Q-factor chiral q-BIC metasurface showcases enhanced intrinsic chiral light–matter interactions and near-unity chiral dichroism. The incorporation of phase-change material $Sb_2S_3$ further endows the metasurface with the ability to dynamically tune the resonant CP emission wavelengths of perovskite. This leads to dynamically tunable chiral emission across a broad spectral range, which significantly enhances the emission of LCP light while effectively suppressing the RCP light emission, demonstrating a remarkable chiral emission enhancement effect. Our metasurface design offers a versatile, dynamically tunable platform with significant potential to advance optical technologies. By enabling precise control of CP emission spectra, the system supports polarization-division multiplexing and enhances chiral response for detecting environmental changes and biomolecules.

See the supplementary material for the supplementary figures about the experimentally measured n and $\kappa$ of the materials, the characteristics of q-BIC with in-plane or out-of-plane symmetry breaking, generation of maximum chirality, optical chirality density of maximum chiral metasurfaces, chiral q-BICs and maximum chirality, and reciprocity calculations of chiral emission.

This work was supported by the National Natural Science Foundation of China under Grant Nos. 92265110, 62174179, and 62204259; the National Key Research and Development Program of China under Grant Nos. 2024YFA1207700, 2022YFA1204100, and 2021YFA1400700; the Key Program of National Natural Science

Foundation of China, Grant No. 12332002; the Science Research Project of Hebei Education Department under Grant No. QN2024128; and the Strategic Priority Research Program of the Chinese Academy of Sciences under Grant No. XDB33020200. This work was also supported by the Micro/Nano Fabrication Laboratory of Synergetic Extreme Condition User Facility (SECUF).

## AUTHOR DECLARATIONS

### Conflict of Interest

The authors have no conflicts to disclose.

### Author Contributions

**Cai Luo:** Conceptualization (equal); Data curation (equal); Formal analysis (equal); Investigation (equal); Methodology (equal); Writing – original draft (equal). **Nannan Hu:** Conceptualization (equal); Investigation (supporting); Validation (supporting). **Jianmei Li:** Conceptualization (equal); Data curation (equal); Formal analysis (equal); Funding acquisition (equal); Investigation (equal); Project administration (equal); Resources (equal); Supervision (equal); Writing – review & editing (equal). **Sha Hu:** Funding acquisition (equal); Project administration (supporting); Resources (supporting). **Ziyi Fu:** Validation (equal); Visualization (equal). **Zhixiang Yu:** Software (supporting); Validation (supporting). **Yanxue Hou:** Funding acquisition (supporting); Project administration (supporting); Validation (supporting). **Aizi Jin:** Resources (supporting); Supervision (supporting). **Baogang Quan:** Funding acquisition (supporting); Project administration (supporting). **Shibing Tian:** Funding acquisition (supporting); Project administration (supporting). **Haifang Yang:** Funding acquisition (supporting); Project administration (supporting). **Geng Li:** Project administration (supporting); Supervision (supporting). **Xiaoyu Zhang:** Data curation (supporting); Funding acquisition (supporting); Supervision (supporting). **Xiaofeng Fan:** Funding acquisition (equal); Project administration (supporting). **Yang Guo:** Conceptualization (equal); Data curation (equal); Formal analysis (equal); Funding acquisition (equal); Methodology (equal); Validation (equal); Writing – original draft (equal); Writing – review & editing (equal). **Changzhi Gu:** Funding acquisition (equal); Project administration (equal).

## DATA AVAILABILITY

The data that support the findings of this study are available from the corresponding authors upon reasonable request.

## REFERENCES

[1]I. C. Seo, Y. Lim, S.-C. An, B. H. Woo, S. Kim, J. G. Son, S. Yoo, Q. H. Park, J. Y. Kim, and Y. C. Jun, "Circularly polarized emission from organic–inorganic hybrid perovskites via chiral fano resonances," ACS Nano **15**(8), 13781–13793 (2021).
[2]Y. Wang, G. Adamo, S. T. Ha, J. Tian, and C. Soci, "Electrically generated exciton polaritons with spin on-demand," Adv. Mater. **37**, 2412952 (2024).
[3]L.-Y. Li, D. Li, X. Dong, Q.-W. Tan, X.-L. Wang, Y.-Z. Wang, and F. Song, "A confined self-assembly approach towards chiral photonic materials with circularly polarized structural colors for information storage and encryption," Chem. Eng. J. **479**, 147669 (2024).
[4]H. K. Bisoyi and Q. Li, "Light-directing chiral liquid crystal nanostructures: From 1D to 3D," Acc. Chem. Res. **47**(10), 3184–3195 (2014).
[5]M. Schadt, "Liquid crystal materials and liquid crystal display," Annu. Rev. Mater. Sci. **27**(1), 305–379 (1997).
[6]H. Lee, M. J. Huttunen, K. J. Hsu, M. Partanen, G. Y. Zhuo, M. Kauranen, and S. W. Chu, "Chiral imaging of collagen by second-harmonic generation circular dichroism," Biomed. Opt. Express **4**(6), 909–916 (2013).
[7]N. Gisin and R. Thew, "Quantum communication," Nat. Photonics **1**(3), 165–171 (2007).
[8]J. Wang, C. Zhang, H. Liu, R. McLaughlin, Y. Zhai, S. R. Vardeny, X. Liu, S. McGill, D. Semenov, H. Guo, R. Tsuchikawa, V. V. Deshpande, D. Sun, and Z. V. Vardeny, "Spin-optoelectronic devices based on hybrid organic-inorganic trihalide perovskites," Nat. Commun. **10**(1), 129 (2019).
[9]J. M. Abendroth, D. M. Stemer, B. P. Bloom, P. Roy, R. Naaman, D. H. Waldeck, P. S. Weiss, and P. C. Mondal, "Spin selectivity in photoinduced charge-transfer mediated by chiral molecules," ACS Nano **13**(5), 4928–4946 (2019).
[10]R. Naaman, Y. Paltiel, and D. H. Waldeck, "Chiral molecules and the electron spin," Nat. Rev. Chem. **3**(4), 250–260 (2019).
[11]S. Ma, J. Ahn, and J. Moon, "Chiral perovskites for next-generation photonics: From chirality transfer to chiroptical activity," Adv. Mater. **33**(47), 2005760 (2021).
[12]B. Ren, G. Yuen, S. Deng, L. Jiang, D. Zhou, L. Gu, P. Xu, M. Zhang, Z. Fan, F. S. Y. Yueng, R. Chen, H.-S. Kwok, and G. Li, "Multifunctional optoelectronic device based on an asymmetric active layer structure," Adv. Funct. Mater. **29**(17), 1807894 (2019).
[13]H. Zeng, P. Lu, X. Li, L. Huang, C. Song, D. Li, I.-K. Lee, S.-T. Kim, Q.-H. Wang, and Y. Liu, "Multiuser computational imaging encryption and authentication with OFDM-assisted key management," Adv. Photonics Nexus **3**(5), 056016 (2024).
[14]J. Tian, G. Adamo, H. Liu, M. Klein, S. Han, H. Liu, and C. Soci, "Optical Rashba effect in a light-emitting perovskite metasurface," Adv. Mater. **34**(12), 2109157 (2022).
[15]J. Tian, G. Adamo, H. Liu, M. Wu, M. Klein, J. Deng, N. S. S. Ang, R. Paniagua-Domínguez, H. Liu, A. I. Kuznetsov, and C. Soci, "Phase-change perovskite microlaser with tunable polarization vortex," Adv. Mater. **35**(1), e2207430 (2023).
[16]Z. Xie, C. Li, K. Murali, H. Yu, C. Liu, Y. Lu, S. A. Maier, M. Bhaskaran, and H. Ren, "Ultrathin BIC metasurfaces based on ultra-low-loss $Sb_2Se_3$ phase-change material," Nano Lett. **25**(1), 251–260 (2025).
[17]X. Sha, K. Du, Y. Zeng, F. Lai, J. Yin, H. Zhang, B. Song, J. Han, S. Xiao, Y. Kivshar, and Q. Song, "Chirality tuning and reversing with resonant phase-change metasurfaces," Sci. Adv. **10**(21), eadn9017 (2024).
[18]S. Hu, C. Wang, S. Du, Z. Han, N. Hu, and C. Gu, "Laser-induced reconfigurable wavefront control with a structured $Ge_2Sb_2Te_5$-based metasurface," Commun. Phys. **7**(1), 346 (2024).
[19]D. Neshev and I. Aharonovich, "Optical metasurfaces: New generation building blocks for multi-functional optics," Light **7**(1), 58 (2018).
[20]M.-S. Hwang, H.-G. Park, Q. Song, and Y. Kivshar, "Advancing nanolasers," Opt. Photonics News **34**(1), 34–41 (2023).
[21]S. Chen, Z. Liu, H. Du, C. Tang, C.-Y. Ji, B. Quan, R. Pan, L. Yang, X. Li, C. Gu, X. Zhang, Y. Yao, J. Li, N. X. Fang, and J. Li, "Electromechanically reconfigurable optical nano-kirigami," Nat. Commun. **12**(1), 1299 (2021).
[22]X. Liu, X. Zhang, W. Dong, Q. Liang, C.-Y. Ji, and J. Li, "Broadband and high-efficiency polarization conversion with a nano-kirigami based metasurface," Sci. Rep. **13**(1), 7454 (2023).
[23]J. Liang, W. Wen, F. Jin, Y. G. Rubo, T. C. H. Liew, and R. Su, "Polariton spin Hall effect in a Rashba–Dresselhaus regime at room temperature," Nat. Photonics **18**(4), 357–362 (2024).
[24]Y. V. Izdebskaya, Z. Yang, V. G. Shvedov, D. N. Neshev, and I. V. Shadrivov, "Multifunctional metasurface tuning by liquid crystals in three dimensions," Nano Lett. **23**(21), 9825–9831 (2023).
[25]S. Hu, Z. Han, S. Du, C. Wang, N. Hu, Z. Fan, X. Huang, and C. Gu, "Nonvolatile switchable Janus metasurface for multi-dimension encoded near- and far-field functionalization," Adv. Funct. Mater. **35**(16), 2419741 (2025).
[26]C. Wang, R. Wang, X. Cheng, X. Hu, and C. Wang, "Passively broadband tunable dual circular dichroism via bound states in the continuum in topological chiral metasurface," ACS Nano **18**(29), 18922–18932 (2024).

[27]M. L. Solomon, J. Hu, M. Lawrence, A. García-Etxarri, and J. A. Dionne, "Enantiospecific optical enhancement of chiral sensing and separation with dielectric metasurfaces," ACS Photonics **6**(1), 43–49 (2019).
[28]K. Voronin, A. S. Taradin, M. V. Gorkunov, and D. G. Baranov, "Single-handedness chiral optical cavities," ACS Photonics **9**(8), 2652–2659 (2022).
[29]T. Shi, Z.-L. Deng, G. Geng, X. Zeng, Y. Zeng, G. Hu, A. Overvig, J. Li, C.-W. Qiu, A. Alù, Y. S. Kivshar, and X. Li, "Planar chiral metasurfaces with maximal and tunable chiroptical response driven by bound states in the continuum," Nat. Commun. **13**(1), 4111 (2022).
[30]Y. Chen, H. Deng, X. Sha, W. Chen, R. Wang, Y.-H. Chen, D. Wu, J. Chu, Y. S. Kivshar, S. Xiao, and C.-W. Qiu, "Observation of intrinsic chiral bound states in the continuum," Nature **613**(7944), 474–478 (2023).
[31]L. Kühner, F. J. Wendisch, A. A. Antonov, J. Bürger, L. de S. Hüttenhofer, L. Menezes, S. A. Maier, M. V. Gorkunov, Y. Kivshar, and A. Tittl, "Unlocking the out-of-plane dimension for photonic bound states in the continuum to achieve maximum optical chirality," Light **12**(1), 250 (2023).
[32]X. Zhang, Y. Liu, J. Han, Y. Kivshar, and Q. Song, "Chiral emission from resonant metasurfaces," Science **377**(6611), 1215–1218 (2022).
[33]M. V. Gorkunov, A. A. Antonov, and Y. S. Kivshar, "Metasurfaces with maximum chirality empowered by bound states in the continuum," Phys. Rev. Lett. **125**(9), 093903 (2020).
[34]H. Qin, Z. Su, M. Liu, Y. Zeng, M.-C. Tang, M. Li, Y. Shi, W. Huang, C.-W. Qiu, and Q. Song, "Arbitrarily polarized bound states in the continuum with twisted photonic crystal slabs," Light **12**(1), 66 (2023).
[35]A. Overvig, N. Yu, and A. Alù, "Chiral quasi-bound states in the continuum," Phys. Rev. Lett. **126**(7), 073001 (2021).
[36]J. K. Gansel, M. Thiel, M. S. Rill, M. Decker, K. Bade, V. Saile, G. von Freymann, S. Linden, and M. Wegener, "Gold helix photonic metamaterial as broadband circular polarizer," Science **325**(5947), 1513–1515 (2009).
[37]C. W. Hsu, B. Zhen, A. D. Stone, J. D. Joannopoulos, and M. Soljačić, "Bound states in the continuum," Nat. Rev. Mater. **1**(9), 16048 (2016).
[38]P. Hu, C. Xie, Q. Song, A. Chen, H. Xiang, D. Han, and J. Zi, "Bound states in the continuum based on the total internal reflection of Bloch waves," Natl. Sci. Rev. **10**(1), nwac043 (2023).
[39]M. Fang, N.-H. Shen, W. E. I. Sha, Z. Huang, T. Koschny, and C. M. Soukoulis, "Nonlinearity in the dark: Broadband terahertz generation with extremely high efficiency," Phys. Rev. Lett. **122**(2), 027401 (2019).
[40]M. Wuttig, H. Bhaskaran, and T. Taubner, "Phase-change materials for non-volatile photonic applications," Nat. Photonics **11**(8), 465–476 (2017).
[41]Q. Wang, E. T. F. Rogers, B. Gholipour, C.-M. Wang, G. Yuan, J. Teng, and N. I. Zheludev, "Optically reconfigurable metasurfaces and photonic devices based on phase change materials," Nat. Photonics **10**(1), 60–65 (2016).
[42]Y. Wang, P. Landreman, D. Schoen, K. Okabe, A. Marshall, U. Celano, H. S. P. Wong, J. Park, and M. L. Brongersma, "Electrical tuning of phase-change antennas and metasurfaces," Nat. Nanotechnol. **16**(6), 667–672 (2021).
[43]I. Sersic, M. A. van de Haar, F. B. Arango, and A. F. Koenderink, "Ubiquity of optical activity in planar metamaterial scatterers," Phys. Rev. Lett. **108**(22), 223903 (2012).
[44]E. Plum, V. A. Fedotov, and N. I. Zheludev, "Optical activity in extrinsically chiral metamaterial," Appl. Phys. Lett. **93**(19), 191911 (2008).
[45]W. Chen, Z. Wang, M. V. Gorkunov, J. Qin, R. Wang, C. Wang, D. Wu, J. Chu, X. Wang, Y. Kivshar, and Y. Chen, "Uncovering maximum chirality in resonant nanostructures," Nano Lett. **24**(31), 9643–9649 (2024).
[46]Q.-M. Deng, X. Li, M.-X. Hu, F.-J. Li, X. Li, and Z.-L. Deng, "Advances on broadband and resonant chiral metasurfaces," npj Nanophotonics **1**(1), 20 (2024).
[47]Y. Tang and A. E. Cohen, "Enhanced enantioselectivity in excitation of chiral molecules by superchiral light," Science **332**(6027), 333–336 (2011).